

Article

An Approach to Nuclear Fusion Utilizing the Dynamics of High-Density Electrons and Neutrals, Part I

Alfred YiuFai Wong * and Chun-Ching Shih

Alpha Ring International Limited, 5 Harris Court, Monterey, CA 93940, USA; shih@alpharing.com

* Correspondence: awong@alpharing.com

Abstract: An approach to achieve nuclear fusion utilizing the formation of high densities of electrons and neutrals is described. The abundance of low energy free electrons produces intense electric fields that reduce the Coulomb barrier in nuclear fusion. Meanwhile, high-density rotating neutrals provide high centrifugal forces to achieve the extreme pressure gradients of electrons and consequent negative electric fields to reduce the ion repulsive Coulombic fields. These high-density neutrals also provide better stability and higher reaction rates. Ion–neutral coupling is responsible for the control of neutral dynamics. Since high-frequency excitations favor the generation of free electrons, pulsed operations are recommended to achieve fusion with higher gains.

Keywords: dynamic electron screening; neutral–neutral fusion; Coulomb barrier reduction; ion–neutral coupling; proton–boron fusion

1. Introduction

In conventional nuclear fusion, the presence of a Coulomb barrier (greater than MeV energies) between interacting nucleons has proved to be very challenging. Conventional nuclear fusion efforts are generally concentrated at overcoming the Coulomb barrier through the confinement of energetic ions of tens to hundreds of keV. By contrast, the Alpha Ring fusion concept is based on changing the height and extent of the Coulomb barrier, increasing the quantum tunneling efficiency, thereby increasing fusion reaction rates. Furthermore, our rotating systems generate significant centrifugal forces to compress pressure profiles which help bring the reactants together.

The first feature of our approach involves using the collective temporal and spatial behaviors of free and low-energy electrons to generate negative electric fields, aimed at overcoming the primary obstacle to fusion, which is the Coulomb repulsion between positively charged nuclei. Poisson's equation governing fields depends only on the difference between electron and ion densities and not on their energies, which allows for a more favorable condition for quantum tunneling between initially low-energy reactants. For example, a highly emissive material, such as lanthanum hexaboride (LaB_6), is heated by rotating neutrals to provide a reservoir of free electrons. At the same time, the radial movement of emitted electrons is blocked by the same rotating high-density ($\sim 10^{26}/\text{m}^3$) neutrals at the outer electrode, such that the free electrons just outside the emitter acquire a high density ($\sim 10^{22}/\text{m}^3$). The oscillatory or collapsing behaviors of these free electrons, such as those existing in resonant plasma waves [1], can further enhance local electron densities. Since fusion events occur in temporal and spatial scales of femtoseconds and femtometers, even high-frequency dynamic electric fields can counteract the repulsive Coulomb electric fields between reactant nuclei, thereby causing fusion.



Academic Editor: Emilio Martines

Received: 19 December 2024

Revised: 24 January 2025

Accepted: 26 January 2025

Published: 31 January 2025

Citation: Wong, A.Y.; Shih, C.-C. An Approach to Nuclear Fusion Utilizing the Dynamics of High-Density Electrons and Neutrals, Part I. *Plasma* **2025**, *8*, 4. <https://doi.org/10.3390/plasma8010004>

Copyright: © 2025 by the authors. Licensee MDPI, Basel, Switzerland. This article is an open access article distributed under the terms and conditions of the Creative Commons Attribution (CC BY) license (<https://creativecommons.org/licenses/by/4.0/>).

To increase the density of reactants, the second feature of our approach involves utilizing centrifugal force created by rotation [2–6]. A highly compressed state, including neutrals, electrons and ions through centrifugal or ponderomotive forces, results in significant fusion events since the fusion rate depends on the product of densities of reactants. The efficiency of using neutrals and ions, instead of requiring a fully ionized plasma, is emphasized in the Alpha Ring’s technology.

The Coulomb barrier is a result of electromagnetic forces which can be modified by appropriate dynamics of negative charges. The wave nature of reactants allows quantum tunneling through this reduced barrier. In Section 2 (Rotating System for Fusion), the authors present a cylindrical rotating plasma immersed in an axial magnetic field. In Section 3 (Coulomb Electric Fields and Potentials Between Two Atoms), it is shown that high gradients of free electrons and negative charges can establish a strong negative potential by centrifugal acceleration. In Section 4 (Enhancement of Fusion Cross Section by Electron Screening), the Schrodinger equation is used to quantify the enhancement of fusion by electron screening, while Section 5 (Enhancement of Fusion Cross Section by Plasma Oscillations) delves into the enhancement of the fusion cross sections by plasma oscillations. Section 6 (Ion-Neutral Coupling) describes how the ion–neutral coupling controls the dynamics of neutrals. Section 7 (Design Parameters of a Rotating Fusion Chamber) provides the design parameters of an example rotating fusion chamber with key performance numbers. Section 8 is the conclusion, and Section 9 is the discussion.

2. Rotating System for Fusion

To bring out the above features of our concept, an Alpha Ring rotation device has been designed, as illustrated in Figure 1. It consists of two coaxial cylinders with a positively biased center electrode and a grounded outer wall. An electric field is imposed across the annular space by applying an electric potential between the inner electrode and the outer electrode (a circular shroud). The gas in the annular space is ionized by the radial plasma current across the annular space. A permanent magnet or a superconducting magnet maintains an axial magnetic field perpendicular to the radial electric field [7]. The $E \times B$ field that exists between the two cylinders generates a Lorentz force which drives charged particles to rotate azimuthally. Charged particles interact with neutrals, leading to the observation of circular motion captured by a fast camera. The absence of a mechanical drive enables the attainment of remarkably high rotation rates, ranging from 10 to 100 kHz. The rapidly rotating, weakly-ionized plasma has a high angular velocity and exerts an extreme pressure on the inner surface of the confining wall through the associated centrifugal force.

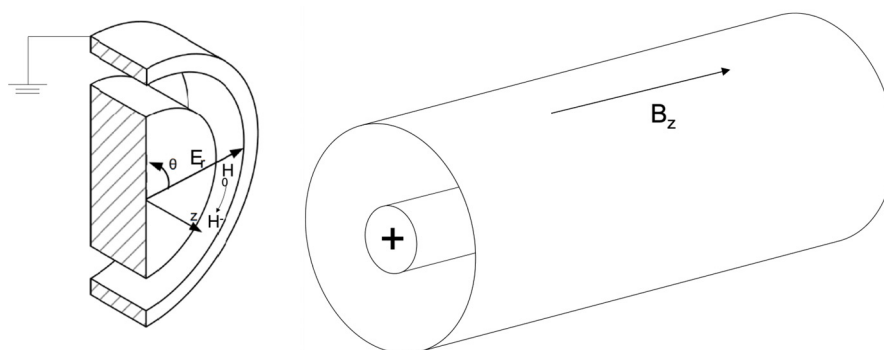


Figure 1. Coaxial cylindrical chamber with radial electric field E_r and axial magnetic field B_z ; hydrogen gas at pressures of 1–4 torr are used.

Concurrently, electrons are emitted from heated LaB_6 emitters mounted on the inner surface of the outer electrode at certain angles. The resultant high-density electron layer

is confined in a thin region created by the centrifugal force and the axial magnetic field. The sharp electron density gradient produces a strong negative electric field that reduces the positive Coulombic repulsion field between reactant nuclei. Hence, the probability of two positively charged nuclei coming in proximity is significantly increased. Rotating neutrals repeatedly pass through the electron-rich layer and strike the inner surface of the outer electrode tangentially which contains the other reactant at high solid density. The rotation configuration allows the same plasma to interact with the wall continuously under centrifugal forces. Efficiency is thus greatly improved, and fusion can take place without requiring an environment of hundreds of million degrees to overcome the natural Coulomb barrier.

The following H-B fusion reaction, as represented by Equation (1)



leads to the production of three alpha particles and an energy release of 8.68 MeV in the form of the kinetic energies of the alphas. A high electron emissive material, lanthanum hexaboride, and hydrogen gas at pressures of 1–4 torr are used.

3. Coulomb Electric Fields and Potentials Between Two Atoms

Instead of imparting extremely high kinetic energy to the fusion reactants to overcome the electrostatic repulsion, Alpha Ring's technology focus on employing an electron-rich region to reduce the Coulomb barrier to fuse two nuclei.

Free electrons in the Alpha Ring rotating device may be viewed as collectively catalyzing the fusion reaction of two nuclei. In early days, around 1957, the muon was described as catalyzing the fusion of a pair of hydrogen and deuterium atoms. Just as one muon can catalyze the fusion process by allowing two reactant nuclei to get closer to one another (~1 pico-meter), billions of free electrons in the vicinity of many reactants catalyze multiple fusion reactions. Effectively, the electrons reduce the energy barrier that prevents the two reactants from coming close enough to react. However, muon catalyzed fusion is not commercially viable, as muons have a much greater mass than electrons and, hence, producing them is much more energetically expensive. In addition, muons have a very short lifetime of approximately 2 microseconds.

By contrast, electrons, unlike muons, can be easily produced by high electron emissive material, such as lanthanum hexaboride, at 1500 K, with high densities by emitters and act collectively to produce a high electric field, especially under compression by a centrifugal acceleration of over a billion times the value of gravitational acceleration on the earth surface. Our recent computer modeling of the rotation process [7] shows the centrifugal force is balanced by a steep pressure gradient of negative charges (electrons, and negatively charged hydrogen ions, H^-). It also shows that fusion reactants experience the attractive force over a much larger distance than just the tunneling region.

From the rotation, the increase in azimuthal velocity v_θ leads to a centrifugal force, which is balanced mainly by the pressure gradient, $\frac{\partial p}{\partial r} = \frac{T \partial n}{\partial r} = \frac{\rho \partial v_\theta^2}{\partial r}$, where p is the pressure, T is the temperature, n is the number density, and ρ is the mass density. It was shown in [7] that, at a velocity of $v_\theta = 1.5 \times 10^5$ m/s near the outer wall, the corresponding centrifugal acceleration is $a_c = 2 \times 10^{11}$ m/s². A density gradient is developed to balance the centrifugal force, leading to a higher density, nearly 1000 times the average density at the outer wall.

4. Enhancement of Fusion Cross Section by Electron Screening

A certain part of the confining wall is composed of electron emitter materials. A surplus of electrons on the inner electrode generates an electron-rich region in proximity to the electrode surface, which rotates in the same direction as the positively charged particles due to the Lorentz force resulting from the potential difference between the inner and outer electrodes. One of the key factors in calculating fusion reaction rates is the cross section, which is usually very small at low energy due to the extremely low penetration factor through the Coulomb barrier around the nucleus. The tunneling through the Coulomb barrier is purely a quantum mechanical phenomenon and can be described by the Coulomb scattering process based on the Schrodinger equation, as follows:

$$-\frac{\hbar^2}{2m}\nabla^2\psi + [V(r) - E]\psi = 0 \tag{2}$$

where $V(r) = Z_1Z_2e^2/r$ is the Coulomb potential between particles of charges Z_1e and Z_2e . Equation (2) can be solved for the Coulomb wave function $\psi(r)$ around the nucleus [8]. Since the nuclear radius ($\sim 10^{-15}$ m) is much smaller than the Coulomb radius ($\sim 10^{-10}$ m), the penetration probability P is related closely to the wave function near $r = 0$, $\psi(0)$, and obtained as follows [8]:

$$P = |\psi(0)|^2 = \frac{2\pi\eta}{\exp(2\pi\eta) - 1} \quad ; \quad \eta = \frac{\alpha Z_1 Z_2 c}{v} \tag{3}$$

where $\alpha = e^2/\hbar c$ is the fine structure constant, v is the particle velocity, c is the light velocity in vacuum, and η is the Sommerfeld constant, which is related to the fine structure constant representing the electromagnetic forces between subatomic charged particles and essentially determining how an atom holds together its electrons. The Sommerfeld constant can be expressed in terms of the particle energy E as follows [8]:

$$2\eta = \sqrt{\frac{E_G}{E}} \quad ; \quad E_G = 2\alpha^2 Z_1^2 Z_2^2 m c^2 \tag{4}$$

where m is the mass in the center of mass frame, E_G is the Gamow energy equivalent to the Coulomb potential at the Bohr nuclear radius, where the Coulomb repulsion is transitioned to the strong interaction regime. Therefore, Gamow energy represents the height of the Coulomb barrier for tunneling, which is proportional to the nuclear charges squared, making it much more difficult to obtain a fusion interaction between high- Z nuclei. Since the reaction rate is proportional to the penetration factor, the fusion cross section is customarily written as follows [9]:

$$\sigma(E) \sim \frac{P(E)}{v} = \frac{S(E)}{E} \frac{1}{\exp\left(\pi\sqrt{\frac{E_G}{E}}\right) - 1} \tag{5}$$

where $S(E)$ is the astrophysical factor, which represents the probability of nuclear reaction after penetration. Usually, $S(E)$ represents a weak dependence on E and can be expanded in power of E^n , where the coefficients of expansion are determined from experiments.

When the penetration probability is small, the fusion cross section can also be calculated from the WKB method [8]. Under this approximation, the barrier penetration factor P can be found as follows:

$$P = \exp\left[-2\int_{r_1}^{r_2} \kappa(r)dr\right] = \exp\left[-\frac{2\sqrt{2m}}{\hbar} \int_{r_1}^{r_2} \sqrt{V(r) - E}dr\right] \tag{6}$$

where $\kappa(r) = \frac{2\sqrt{2m}}{\hbar} \sqrt{V(r) - E}$ is the wave decay constant in the barrier region and the integral covers the radial range where $E < V(r)$. For unscreened Coulomb potential, $V(r) = Z_1 Z_2 e^2 / r$, the integral can be carried out exactly and we have the penetration probability as follows [8]:

$$P = \exp \left\{ -\frac{2\pi Z_1 Z_2 e^2}{\hbar v} \left[1 - \frac{2}{\pi} \left(\sin^{-1} \sqrt{\zeta} + \sqrt{\zeta - \zeta^2} \right) \right] \right\} \quad (7)$$

where $\zeta = \frac{E}{U_{pk}}$ and U_{pk} is the peak potential barrier. In the case of small E , ζ is negligible and

$$P \approx \exp \left(-\frac{2\pi Z_1 Z_2 e^2}{\hbar v} \right) = \exp \left(-\pi \sqrt{\frac{E_G}{E}} \right) \quad (8)$$

Here P has the same exponential dependence on energy E , as given in Equation (3), when E is much smaller than E_G ($\eta \gg 1$, a generally valid approximation for most cases). It is important to note that this same potential also governs the radiative decay as pointed out by Gamow, Gurney, and Condon [10,11].

By creating an external negative potential in addition to the positive Coulomb potential, the height and width of the overall Coulomb barrier to be penetrated is reduced. This external potential is typically generated by a layer of negative charges, with a characteristic distance longer than the separation between the nuclei. This property is crucial to quantum tunneling and, consequently, to fusion. The total potential is thus the sum of Coulomb potential and the screening potential, which is the integration of the screening field $F_s(r)$ over the whole space. Accounting for this effect, the Schrodinger equation becomes the following:

$$-\frac{\hbar^2}{2m} \nabla^2 \psi + [V(r) - U(r) - E] \psi = 0 \quad (9)$$

And the barrier penetration factor P' can be found as follows:

$$P = \exp \left[-\frac{2\sqrt{2m}}{\hbar} \int_{r_1'}^{r_2'} \sqrt{V(r) - U(r) - E} dr \right] \quad (10)$$

Here, the new integration range of integration r_1' to r_2' is over the region where $V(r) - U(r) > E$. In general, $U(r)$ has a negligible variation within this very small range and can be represented by a constant U_s . For the case of screening by a charge sheet, $U_s = \frac{e^2 n_{se} L}{2\epsilon_0}$ is given, as shown in the caption of Figure 2. Since the result in Equation (7) is independent of r_1 and r_2 , we can neglect the new values of r_1' and r_2' in Equation (10). Under this approximation, Equation (10) is identical to Equation (6) if E in Equation (6) is replaced by $(E + U_s)$. As a result, we can use a similar formula as in Equation (3) and obtain penetration probability with screening effects as follows:

$$P = \pi \sqrt{\frac{E_G}{E + U_s}} \frac{1}{\exp \left(\pi \sqrt{\frac{E_G}{E + U_s}} \right) - 1} \quad (11)$$

And the screened cross section, as in Equation (5), can be written as follows:

$$\sigma(E, U_s) = \frac{S(E + U_s)}{E + U_s} \frac{1}{\exp \left(\pi \sqrt{\frac{E_G}{E + U_s}} \right) - 1} \quad (12)$$

The screening energy can thus affect the fusion cross section, especially when it is close to or higher than the particle energy. Figure 3 shows the cross sections for a p-¹¹B

reaction for screening energies up to $U_s = 45$ keV, using Gamow energy $E_G = 2.29$ MeV for p-B and the following empirical astrophysical factor, $S(E) = C_0 + C_1E + C_2E^2$. For the p-B cross section, the values of those three coefficients are as follows: $C_0 = 195$ MeV-barn, $C_1 = 241$ barn, and $C_2 = 231$ barn/MeV [12]. The resonant structure near $E = 148$ keV, as shown in [11], is neglected because the energy of our interest is far away from 148 keV.

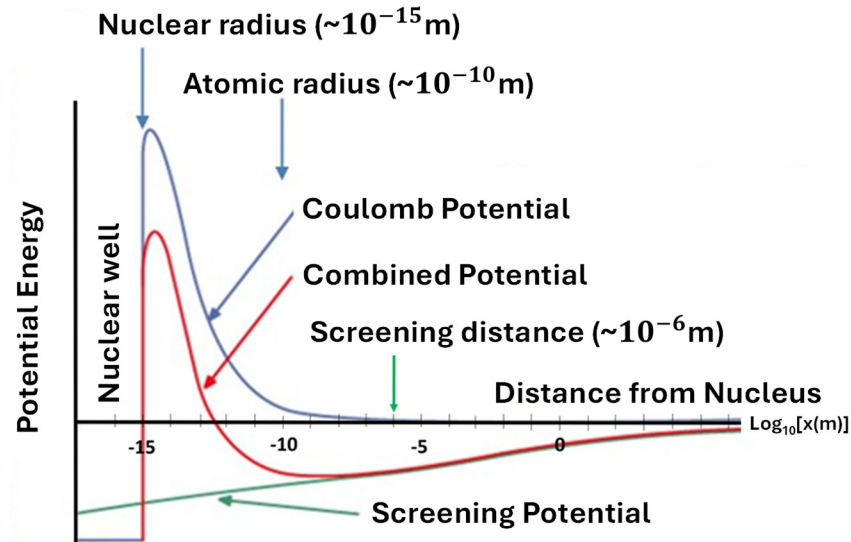


Figure 2. Schematic drawing of Coulomb barrier reduction in the presence of high-density electrons in the vicinity of two nuclei. The total tunneling region represented by the red trace is made smaller and narrower due to the negative potential generated by negative charges (the green line). The probability of fusion is enhanced because of increased tunneling through this modified region. The green line is based on the on-axis electric potential of a charge disk of radius R and surface electron density n_{se} : $U(x) = \frac{e^2 n_{se}}{2\epsilon_0} (|x| - \sqrt{x^2 + R^2})$. It is expected that the screening potential would start at a negative value at $x = 0$ and increase linearly when $x \ll R$, a typical situation in our fusion set-up since the extent of the charge sheet is much larger than the starting position of the projectile, L . In this case, the screening energy can be found as $U_s = U(L) - U(0) \approx \frac{e^2 n_{se} L}{2\epsilon_0}$. The scales are relative for the purpose of illustration only. All potentials are gradually reduced to zero when the separation approaches infinity.

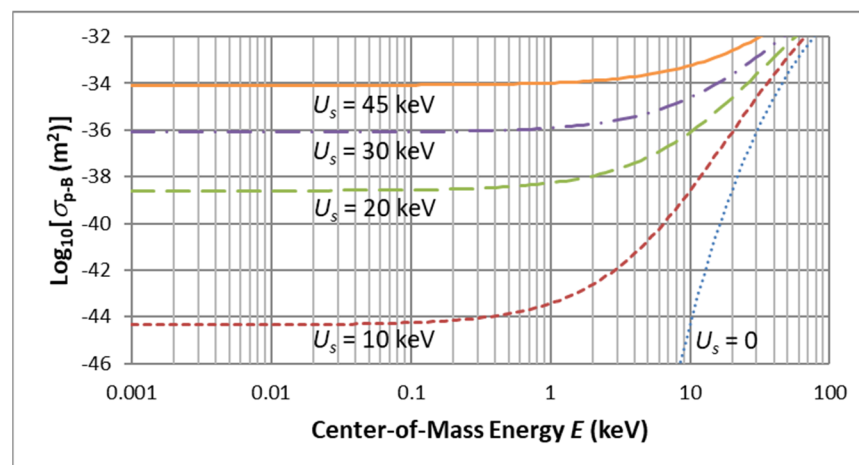


Figure 3. $p\text{-}^{11}\text{B}$ cross section as a function of particle energy for screening electron densities up to $U_s = 45$ keV. The cross section near $E = 1$ eV grows over 10 orders of magnitude (from 10^{-44} to 10^{-34} m^2) over the U_s range of 10 to 45 keV.

Without screening ($U_s = 0$), the cross sections drop quickly when the particle energy goes below a few tens of keV. With the screening effect, the cross sections turn nearly flat below a few keV's of E because the screening energy dominates over the particle energy in this region. The cross section rises very quickly with the screening energy (from 10^{-44} to $\sim 10^{-34}$ m² as U_s increases from 10 to 45 keV). The strong ion–neutral coupling in the rotation chamber is responsible for bringing neutrals to acquire rotation energies of 1–20 eV. In the following section, we will show how to create a fusion environment with high screening energies and compare the effect to other known processes, such as muon-catalyzed fusion [13,14].

In the preceding section, we have demonstrated the significance of screening energy in determining the screened cross section. By modulating the electron density distributions surrounding the positive Coulomb potential, a negative potential can be created, and the corresponding screening energy can be evaluated. It should be emphasized that the collective electron motions generate the electric field that leads to the screening effect, and the physical presence of electrons between the fusing nuclei is not necessary.

Bound electrons around the nucleus can provide a certain degree of screening for the incoming projectile. However, their charge distribution is basically fixed, and the screening effect was found to be limited, usually from 27 eV (for the hydrogen atom) to, at most, a few hundred eVs. On the other hand, the muon in the muon–hydrogen reaction is also bounded by the nucleus. However, due to its large mass (~ 200 times the electron mass), it brings the two nuclei in the hydrogen molecule much closer and thus facilitates higher possibilities for fusion. The screening energy for the muon–hydrogen is in the vicinity of 5 keV. However, an efficient muon fusion process is difficult to achieve due to its short lifetime, around 2 microseconds [14]. Since bound electrons cannot provide a sufficient screening effect for the fusion process [15,16], a different approach using unbound (free) electrons is explored in the next section.

Screening by Dynamic Free Electron Oscillations

High-density free electrons are created when there are high frequency excitations which ions cannot follow due to their mass. In the case when there is a thin slab layer of electrons created because of the high centrifugal force, the resultant negative electric field will reduce the Coulomb barrier. We emphasize the utilization of repetitive excitation of electron emitters through electrical means. Given the ultrafast timescale of femtoseconds for the fusion process, the impact of such electron interactions will manifest within the critical layer.

As an example, we consider a plasma wave with the sinusoidal form of

$$n(x) = n_0 + n_1 \cos\left(\frac{2\pi x}{\Lambda}\right) \tag{13}$$

where n_1 is the plasma wave amplitude and Λ is the wavelength. From Poisson's equation, the corresponding electric potential energy can be found to be as follows:

$$V(x) = \frac{n_1 e^2 \Lambda^2}{\pi} \cos\left(\frac{2\pi x}{\Lambda}\right) \tag{14}$$

The amplitude of the potential variation is thus the screening energy, which can be written as follows:

$$U_s = \frac{n_1 e^2 \Lambda^2}{\pi} \approx 4.6 \times 10^{-10} [eV \cdot m] n_1 \Lambda^2 \tag{15}$$

For a typical plasma wave induced by a visible or infrared laser, the wavelength is $\Lambda \sim 10^{-6}$ m [17]. In this case, the screening potential is $U_s = 4.6$ keV for a plasma wave

amplitude of $n_1 = 10^{25} \text{ m}^{-3}$. This energy is comparable to the screening energy for the muon-catalyzed hydrogen fusion (5 keV). Therefore, we expect an electron plasma wave of amplitude $\sim 10^{25} \text{ m}^{-3}$ around a hydrogen atom would result in a cross section close to the muon-catalyzed fusion. Apparently, such plasma waves should be easier to produce than the short-lived muons. The nonlinear collapse [18,19] of plasma waves can lead to the compression of even smaller spatial scales. These highly localized oscillating electric fields lead to ponderomotive forces that are proportional to the gradient of field intensities. These forces compress positive ions together and help to lower the Coulomb barrier between positively charged nuclei.

5. Enhancement of Fusion Cross Section by Plasma Oscillations

In fusion research, it is difficult to confine ions due to their high kinetic energy and the low density of reactants. To address this issue, we propose a new concept for fusion interactions based on plasma oscillations between two oppositely charged species [20], rather than between cations. This concept takes advantage of the overall neutrality of charges, bringing anions and cations together to oscillate with each other in a more stable manner than in a single-component plasma. Oscillations mean that anions and cations meet with each other repeatedly, increasing the probability of fusion reactions.

The high fields and potential generated by oscillating high-density plasmas provide the necessary screening energy to enhance fusion reactions. Since the fusion reactants are also the oscillating media, the cycling motion of the ions ensures that their interactions are repeated at high frequencies, resulting in a higher efficiency of the process.

6. Ion–Neutral Coupling

Although neutrals do not experience electrical and/or magnetic forces, their rotation in the confinement region is dependent on their interaction with charged particles (Figure 4). This interaction is facilitated by an ion–neutral coupling process, whereby a small number of charged particles transfer motion to the surrounding neutral particles. More importantly rotating neutrals are influenced by the centrifugal force; acceleration as high as 10^9 g has been observed.

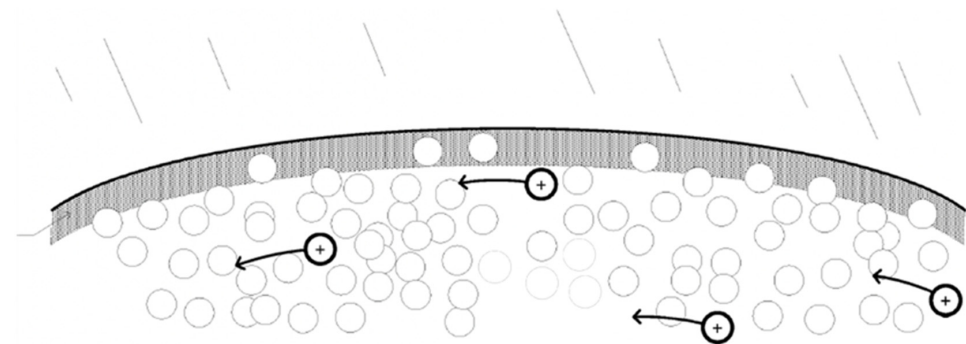


Figure 4. The majority of neutral atoms, accompanied by a smaller proportion of ions and electrons, inhabit the annular region within the cylindrical casing.

B. Lehnert [21] produced a partially ionized plasma centrifuge, where the motion of gas mixture is driven by a small amount of rotating plasma. Plasma motion is controlled by externally imposed crossed electric and magnetic fields; that is, an imposed radial electric field and current, via an applied voltage, between a cylindrical pair of electrodes and an imposed perpendicular axial magnetic field. Lehnert also reported high rotational velocities, large separation degrees, and stable velocity profiles could be attained at comparatively small power losses, within certain parameter ranges.

An outward electric field (E) coexists with an axial magnetic field (B) within the annular cavity. This magnetic field aligns perpendicularly to the radial electric field lines and parallels the surface of the cylindrical electrode. Under the influence of the cross-field phenomenon ($E \times B$), charged particles, ions and electrons, undergo radial motion directed towards the outer cylindrical surface. This radial movement, perpendicular to the axial magnetic field, creates a Lorentz force that propels ions into azimuthal rotational motion, orthogonal to both the radial electric field (E) and axial magnetic field (B). Frequent high-frequency collisions between ions and neutral atoms result in their collective motion. Ions within the annular space experience electrostatic forces due to electric fields, where a relatively small number of ions suffice to drive numerous neutrals via ion–neutral coupling. Ions, serving to induce neutral rotation, can originate from various mechanisms, such as inductive or capacitive coupling. This coupling aligns the co-rotation of neutrals with positively charged particles. Under centrifugal compression, ions, electrons, and neutrals are pressed against the outer cylindrical surface. The aim is to position fusion at the chamber’s outer edge, where electrons, neutrals, and ions converge due to substantial centrifugal acceleration ($>10^9$ g). Centrifugal compression operates on the combined co-rotating ensemble of particles, including neutral atoms, positive ions, and electrons, compressing them into a thin, densely populated rotating layer of fusion reactant nuclei and trapped electrons. This thin, centrifugally compressed layer generates a significant electric field, exerting its influence on the desired reactants.

The process of ion–neutral coupling and the collaborative oscillations among reactant particles lead to a reduction in space charge and associated instabilities. When neutrals are included in the overall fusion reactions, the gain is higher than using the charge species alone.

The following equations describe how neutrals through their frequent collisions with ions can be made to follow the external electromagnetic excitations.

$$Mn_i \frac{\partial \underline{v}_i}{\partial t} = qn_i(\underline{E} + \underline{v}_i \times \underline{B}) - \nabla p_i + P_{ie} \tag{16}$$

$$mn_e \frac{\partial \underline{v}_e}{\partial t} = -qn_e(\underline{E} + \underline{v}_e \times \underline{B}) - \nabla p_e + P_{ei} \tag{17}$$

where M and m are the mass of ion and electron, $n_{i,e}$ are the densities of ions and electrons, $v_{i,e}$ are the velocities of ions and electrons, $p_{i,e}$ are the momentums of ions and electrons, \underline{E} is the electric field, \underline{B} is the magnetic field, and the coupling term, P_{ie} , is the momentum change due to ion–electron interaction (note that $P_{ie} = -P_{ei}$).

Neglecting the viscosity tensor and $(\underline{v} \cdot \nabla)\underline{v}$ terms and adding Equations (16) and (17), the interaction terms are canceled, and we have the following:

$$\frac{\partial}{\partial t}(Mn_i \underline{v}_i + Mn_e \underline{v}_e) = q[(n_i \underline{v}_i - n_e \underline{v}_e) \times \underline{B}] - \nabla(p_i + p_e) \tag{18}$$

Equation (18) can be written as follows:

$$\rho n_e \underline{v}_e = \underline{j} \times \underline{B} - \nabla p \tag{19}$$

where $\rho = n_i M + n_e m = n(M + m)$ is the combined ion–electron density, and the average velocity and effective electric current are (assuming $n \sim n_i \sim n_e$).

$$\underline{v} = \frac{1}{\rho}(n_i M \underline{v}_i + n_e m \underline{v}_e) \approx \frac{M \underline{v}_i + m \underline{v}_e}{M + m} \tag{20}$$

$$\underline{j} = q(n_i \underline{v}_i - n_e \underline{v}_e) \approx qn(\underline{v}_i - \underline{v}_e) \tag{21}$$

Now, consider the interactions between the charge current and the neutrals. Their equations can be written as follows:

$$\text{Neutrals } Mn_0 \frac{\partial v_0}{\partial t} = -\nabla p_0 + P_{ni} \tag{22}$$

$$\text{Charged } \rho \frac{\partial v}{\partial t} = \underline{j} \times \underline{B} - \nabla p_{ie} + P_{in} \tag{23}$$

Equations (22) and (23) show that the neutrals can be influenced by $\underline{j} \times \underline{B}$ force through collisions with charges represented by P_{ni} term. Computer simulations [7] have yielded results indicating the possibility of accelerating neutrals to energies in the keV range. This suggests that significantly higher fusion cross sections can be achieved compared to the existing method.

7. Design Parameters of a Rotating Fusion Chamber

The design parameters for a rotating device are given in Table 1. Note that this case is more conservative than the report in [7]. This design has a lower wall velocity (63 km/s vs. 150 km/s in the simulation [7]). We expect the fusion output will increase with higher rotating frequency.

Table 1. Design parameters for a rotating fusion device.

	Parameter	Value	Unit	Comment
1	Rotating frequency, f	10^5	RPS	Input
2	Radius of rotation chamber, R	0.1	m	Input
3	Gas temperature, T	0.09	eV	At 1000° K
4	Initial gas pressure, P_i	3	torr	Input
5	Gas velocity near outer wall, v	6.28×10^4	m/s	$v = 2\pi Rf$
6	Centrifugal acceleration, a	3.95×10^{10}	m/s ²	$a = v^2/R$
7	Energy of H ₂ near outer wall, E	41.22	Joules	$E = mv^2/2$
8	Gas compression ratio, C	478		$C = E/kT$
9	Gas pressure near outer wall, P_w	1.89	atm	$P_w/P_i = C$
10	Initial gas density, n_i	2.90×10^{22}	1/m ³	$n_i = P_i/kT$
11	Gas density near outer wall, n_w	1.39×10^{25}	1/m ³	$n_w/n_i = C$
12	Density of gaseous boron, n_b	1×10^{25}	1/m ³	Input
13	Neutral layer width near wall, L_n	209.2	μm	$R/L_n = C$
14	Electron layer width near wall, L_e	1	μm	Input
15	2-D electron layer density, n_{2d}	1.39×10^{17}	1/m ²	$n_{2d} = n_w L_e$
16	Screening electric field, E_s	1.25×10^9	V/m	$E_s = n_{2d}/\epsilon$
17	Field interaction length, L_i	10	μm	Input
18	Screening energy, U_s	12.51	keV	$U_s = E_s * L_i$
19	p-B reaction cross section, σ	5.5×10^{-15}	barn (10 ⁻²⁸ m ²)	From Equation (12)
20	Reaction rate per unit volume, κ/V	4.8×10^{12}	1/m ³ /s	$\kappa/V = \sigma v n_1 n_2$
21	Device active length, L_a	0.01	m	Input
22	Total reaction volume, V	1.3×10^{-6}	m ³	$V = 2\pi RL_a$
23	Total reaction rate, κ	6.3×10^6	1/s	$\kappa = (\kappa/V) V$

The rotating frequency of the medium in the chamber (radius of 10 cm), which depends on the radial electric field and axial magnetic field, is set at 10^5 rounds per second (RPS). The original gas density and temperature are assumed to be 3 torr and 1000 degrees, respectively. As the gas rotates, the centrifugal force reaches 10^{10} m/s², which presses the gas to the wall with a compression ratio close to 500. The gas pressure near the wall reaches 1.89 atm. This high neutral density can block the electrons from radial expansion. As a result, the electron layer has a density of about 0.08 C/m², which generates a field of 1.25 GV/m. The screening energy can thus be 12.5 keV, assuming the interaction length is 10 mm. This screening energy enhances the p-B cross section to about 5.5×10^{-43} m² and results in a reaction rate of 6×10^6 per second in the chamber of 1 cm long. This level of reaction rate is only possible with the screening process as described. We have chosen high neutral pressures because the electrons can attach easily to the atomic H₀ to form H⁻ in the reaction $H_0 + e \rightarrow H^- + 0.75$ eV. In addition, low temperature electrons can be produced easily, and they do not radiate into the surroundings. The final fusion rate depends on the densities of H⁻ and ¹¹B⁺. The scaling up of the device to higher outputs will be discussed in Part II paper.

8. Conclusion

Our approach of utilizing the dynamics of high-density free electrons and neutrals has shown promising results in achieving fusion reactions with a higher ratio of released energy compared to the incident energy [22]. This contrasts with the concept of using extremely high-power pulsed lasers or ion beams to enhance tunneling probabilities [23]. A 1-D analysis by another group has shown that the required dynamic field strength to help tunnel through a square barrier of 0.2 nm width is over 10^{16} V/m at a frequency near 10^{17} Hz [24]. This extremely high field is necessary because the effect is limited only to the tunneling region of 2 angstroms, not considering its possible influence before the reactants reach each other's nucleus. The collective dynamics of free electrons in our approach play a significant role in reducing the Coulomb barrier through the generation of net negative charges and the consequent long-range negative potentials and fields. The required field strength is much lower because of the longer interaction distance. We have presented a number of time-dependent methods to enhance the number of free electrons to provide negative electric fields. A comparison between bound electrons and free electrons based on Poisson's equation shows that free electrons can be used more effectively because bound electrons are constrained by their orbit structures. Our theory considers low-energy electrons and H⁻ to lower the Coulomb barrier. Slabs of free electrons and negative ions can act over a long distance from the fusion target to enhance the screening process.

9. Discussion

We have relied on Poisson's equation that negative electric fields are derived from the number of negative charges present and not from the energy of these charges. A high number of neutrals increases the number of negative charges through electron attachments provided the temperatures are maintained below 0.75 eV. For this reason, our system operates at low temperatures and high densities. High neutral densities also contribute to strong plasma stability and increased centrifugal forces, in addition to high fusion reaction rates. If fusion is to be commercialized it must be designed on a small scale with a net gain greater than unity.

This manuscript (part 1) lays out the general approach towards a table-top and miniaturized model. Experimental support will be described in a second manuscript (part 2) with new diagnostics to demonstrate that fusion does take place at low temperatures if collective plasma effects are considered.

Author Contributions: Conceptualization, A.Y.W.; data curation, A.Y.W. and C.-C.S.; formal analysis, A.Y.W. and C.-C.S.; funding acquisition, A.Y.W.; investigation, A.Y.W.; methodology, A.Y.W.; project administration, A.Y.W.; resources, A.Y.W.; software, C.-C.S.; supervision, A.Y.W.; validation, A.Y.W. and C.-C.S.; visualization, A.Y.W.; writing—original draft, A.Y.W.; writing—review and editing, A.Y.W. and C.-C.S. All authors have read and agreed to the published version of the manuscript.

Funding: This research was fully funded by the investors of Alpha Ring International.

Institutional Review Board Statement: Not applicable.

Informed Consent Statement: Not applicable.

Data Availability Statement: The original contributions presented in this study are included in the article. Further inquiries can be directed to the corresponding author(s).

Acknowledgments: We would like to express our sincere gratitude and appreciation to Peter Hsieh and Zhifei Li for their exceptional contributions and tireless discussion towards this paper. Their expertise and dedication have been instrumental in bringing advances to this concept. We are grateful to J. Chen, A. Chen, T. Cremer, M. Guffey, A. Gunn, G. Paskalov, J. Scharer, and B. Mei for their contributions to the operation of our laboratories, and to W. Chai, P. Liu, K. Yanev, and C. Wong for their valuable encouragement and advice. We acknowledge the financial support provided by Alpha Ring international Ltd.

Conflicts of Interest: Author Alfred YiuFai Wong and Chun-Ching Shih are employed by Alpha Ring International Limited (USA). The authors declare no conflicts of interest. The funders had no role in the design of this study; in the collection, analyses, or interpretation of data; in the writing of the manuscript; or in the decision to publish the results.

References and Note

1. Wong, A.Y.; Cheung, P.Y. Three-Dimensional Self Collapse Langmuir Waves. *Phys. Rev. Lett.* **1984**, *52*, 1222–1225. [[CrossRef](#)]
2. Lee, K.H.; Lee, L.C.; Wong, A.Y. Acceleration of ions and neutrals by a traveling electrostatic wave. *Phys. Plasmas* **2018**, *25*, 023113. [[CrossRef](#)]
3. Wong, A.Y.; Jassby, D.L. Collisionless Wave-Particle Interactions Perpendicular to Magnetic Field. *Phys. Rev. Lett.* **1972**, *29*, 41–45. [[CrossRef](#)]
4. Wong, A.Y. Rotating High-Density Fusion Reactor for Aneutronic and Neutronic Fusion. U.S. Patent US9245654B2, 2 June 2016.
5. Wong, A.Y. System and Method for Remediation of Selected Atmospheric Conditions and System for High Altitude Telecommunications. U.S. Patent US5678783A, 21 October 1997.
6. Wong, A.Y. System and Method for Remediation of Selected Atmospheric Conditions. U.S. Patent US5912396A, 15 June 1999.
7. Wong, A.Y.; Lee, K.H.; Lee, L.C. Simulation of dynamics of rotating weakly ionized plasmas. *Phys. Plasmas* **2024**, *31*, 013101. [[CrossRef](#)]
8. Schiff, L.I. Section 21 Scattering by a Coulomb Field, Section 34 The WKB Approximation. In *Quantum Mechanics*, 3rd ed.; McGraw-Hill, Inc.: New York, NY, USA, 1968.
9. Ishimaru, S.; Kitamura, H. Pycnonuclear reactions in dense astrophysical and fusion plasmas. *Phys. Plasmas* **1999**, *6*, 2649–2671. [[CrossRef](#)]
10. Gamow, G. On the Quantum Theory of the Atomic Nucleus. *Z. Phys.* **1928**, *51*, 204–212. [[CrossRef](#)]
11. Gurney, R.W.; Condon, E.U. Quantum Mechanics and Radioactive Disintegration. *Nature* **1928**, *122*, 439–440. [[CrossRef](#)]
12. Becker, H.W.; Rolfs, C.; Trautvetter, H.P. Low-energy cross sections for $^{11}\text{B}(p, 3\alpha)$. *Z. Phys. A-Hadron. Nucl.* **1987**, *327*, 341–355.
13. Alvarez, L.W.; Bradner, H.; Crawford, F.S., Jr.; Crawford, J.A.; Falk-Vairant, P.; Good, M.L.; Gow, J.D.; Rosenfeld, A.H.; Solmitz, F.; Stevenson, M.L.; et al. Catalysis of Nuclear Reactions by μ Mesons. *Phys. Rev.* **1957**, *105*, 1127–1128. [[CrossRef](#)]
14. Jackson, J.D. Catalysis of Nuclear Reactions between Hydrogen Isotopes by μ -Mesons. *Phys. Rev.* **1957**, *106*, 330–339. [[CrossRef](#)]
15. Angulo, C.; Engstler, S.; Raimann, G.; Rolfs, C.; Schulte, W.H.; Somorjai, E. The effects of electron screening and resonances in (p, α) reactions on ^{10}B and ^{11}B at thermal energies. *Z. Phys. A-Hadron. Nucl.* **1993**, *345*, 231–242. [[CrossRef](#)]
16. Barker, F.C. Electron screening in reactions between light nuclei. *Nucl. Phys. A* **2002**, *707*, 277–300. [[CrossRef](#)]
17. Huang, X. and El-Sayer, M.A. Gold Nanoparticles: Optical Properties and Implementation in Cancer Diagnosis and Photothermal Therapy. *J. Adv. Res.* **2010**, *1*, 13–28. [[CrossRef](#)]
18. McFarland, M.D.; Wong, A.Y. Localized Langmuir Field Structures Induced by Sharp Density Gradients. *Phys. Rev. Lett.* **1998**, *80*, 5540–5543. [[CrossRef](#)]

19. Zakharov, V.E. Collapse of Langmuir waves. *Sov. Phys. JETP* **1972**, *35*, 908–914.
20. Wong, A.Y.; Shih, C.C. Enhancement of Nuclear Fusion in Plasma Oscillation Systems. *Plasma* **2022**, *5*, 176–183. [[CrossRef](#)]
21. Lehnert, B. Rotating Plasmas. *Nucl. Fusion* **1971**, *11*, 485. [[CrossRef](#)]
22. Wong, A.Y.; Chen, J.Z.; Guffey, M.J.; Gunn, A.; Mei, B.; Shih, C.C.; Wang, Q.; Zhang, Y. Influence of Electromagnetic Fields on Nuclear Processes. *arXiv* **2020**, arXiv:2011.05385.
23. Kohlfurst, C.; Queisser, F.; Schützhold, R. Dynamically assisted tunneling in the impulse regime. *Phys. Rev. Res.* **2021**, *3*, 033153. [[CrossRef](#)]
24. Ryndyk, D.; Kohlfürst, C.; Queisser, F.; Schützhold, R. Dynamically assisted tunneling in the Floquet picture. *Phys. Rev. Res.* **2024**, *6*, 023056. [[CrossRef](#)]

Disclaimer/Publisher’s Note: The statements, opinions and data contained in all publications are solely those of the individual author(s) and contributor(s) and not of MDPI and/or the editor(s). MDPI and/or the editor(s) disclaim responsibility for any injury to people or property resulting from any ideas, methods, instructions or products referred to in the content.